IEEE Access
Multidisciplinary | Rapid Review | Open Access Journal

Received April 9, 2020, accepted April 22, 2020, date of publication April 27, 2020, date of current version May 13, 2020.

Digital Object Identifier 10.1109/ACCESS.2020.2990710

Pilot Sequence Design for mmWave Cellular Systems With Relay Stations in the Presence of Blockage

YEONG JUN KIM[1], QASIM SULTAN[2], AND YONG SOO CHO[2], (Senior Member, IEEE)
[1]LG Electronics, Seoul 150-721, South Korea
[2]Department of Electrical and Electronics Engineering, Chung-Ang University, Seoul 06974, South Korea

Corresponding author: Yong Soo Cho (yscho@cau.ac.kr)

This work was supported by the National Research Foundation of Korea (NRF) Grant funded by the Korean Government (MSIT) under Grant 2018R1A4A1023826 and Grant 2018R1A2B2002621.

ABSTRACT Due to short wavelength and weak diffraction ability, millimeter-wave (mmWave) signals are highly susceptible to blockage, which results in significant degradation in received signal power. As a possible solution for overcoming the blockage problem in millimeter-wave communication systems, the deployment of a relay station (RS) has been considered in recent years. In this paper, we discuss the problems to be considered in a relay-assisted mmWave cellular system based on orthogonal frequency division multiplexing. We describe a frame structure and a pilot-based training method to achieve efficient RS selection during blockage. In addition, a method designed to overcome the inter-symbol interference problem caused by different symbol time offsets of pilot signals received from adjacent RSs in the relay-assisted mmWave cellular system is discussed. Then, we propose two different types of pilot sequences that allow a mobile station to distinguish among the pilot sources in multi-cell multi-relay environments: pilot signals based on the Zadoff-Chu sequence (PS1) and pilot signals based on the m-sequence (PS2). The correlation property of PS2 is derived and compared with that of PS1 and another sequence (Gold sequence). Simulations are performed using a blockage model to verify the properties, constraints, and advantages and disadvantages of the proposed pilot sequences in RS-assisted mmWave cellular systems.

INDEX TERMS Blockage, cellular system, mmWave, pilot sequence design, relay.

I. INTRODUCTION

The widespread use of wireless smart devices for various applications and services has given rise to a significant increase in mobile data traffic. Millimeter-wave (mmWave) communication is an enabling technology that has found use in many applications, such as cellular networks, vehicular communication, Unmanned aerial vehicle (UAV) communication, positioning, and virtual reality (VR) [1]–[7]. Highly directional beam-forming antennas are necessary at both the base station (BS) and mobile station (MS) to compensate for high attenuation in the mmWave frequency band and to extend the transmission range [8]. The short wavelength of the mmWave frequency enables the easy installation of antenna arrays in an MS. The mmWave frequency is being considered for mobile broadband communications in 5G New Radio (5G NR) and the 5G Special Interest Group (5G SIG), all of which are based on orthogonal frequency division multiplexing (OFDM) [9]–[11]. Although mmWave communication has great potential for high data rate transmission, its characteristics differ significantly from those of conventional wireless technologies. The disadvantages of mmWaves include their short propagation and low penetration. MmWave systems have a significantly lower operating range than microwave systems because of large path loss and their susceptibility to environmental factors. Owing to its weak diffraction ability and severe penetration loss, mmWave communication is highly susceptible to blockage. The deployment of relay stations (RSs) in microwave communication systems has been considered with the aim of extending the coverage and bypassing obstacles, because these RSs provide an alternative path for signal transmission from the source to the destination [12]–[15]. This may also be a possible solution to overcome the blockage

The associate editor coordinating the review of this manuscript and approving it for publication was Zhenyu Xiao.

and coverage problems in mmWave communication systems. When an MS is connected to an RS in the same cell and moves around within the cell, it does not require a handover procedure.

The potential benefits of deploying RSs in mmWave networks have been studied [16]–[18]. Xie *et al.* [16] demonstrated that RSs can be effectively used in mmWave cellular networks to help alleviate blockages and provide line-of-sight (LoS) links when blockage occurs. With the assistance of RSs, more LoS links are expected and the network signal-to-noise ratio (SNR) or signal-to-interference-noise ratio (SINR) performance can be improved significantly. Lan *et al.* [17] proposed a deflecting routing scheme to improve the effective throughput by sharing time slots for the direct path with the relay path in mmWave wireless personal area networks. Biswas *et al.* [18] investigated the coverage probability and transmission capacity of relay-assisted outdoor mmWave networks using stochastic geometry tools. Yang and Xiao [19] studied the impact of the beamwidth and self-interference coefficient on maximum achievable rates for a two-hop relaying mmWave system.

The basic concept of relay-assisted mmWave networks has been extended to either improve the performance or to reduce the computational complexity [20]–[25]. Abbas and Hamdi [20] examined the impact of employing multiple RSs and larger arrays on the overall performance. Belbase *et al.* [21] proposed a two-way relay scheme to double the spectral efficiency by accomplishing bi-directional data exchange in two time slots, as opposed to a one-way relay scheme where bi-directional data exchange between two end users requires four time slots. Xue *et al.* [22] proposed a joint source and relay precoding design scheme for mmWave systems with multiple antennas. The rate maximization problem with the per antenna power constraints is solved while taking into account the computational complexity and sparse characteristics of mmWave channels. Jagyasi and Ubaidulla [23] proposed device-to-device (D2D) relaying and low-complexity mmWave system architecture to alleviate the blockage problem in mmWave bands and improve user experience consistency. Wu *et al.* [24] discussed two-hop D2D relaying for mmWave cellular networks when infrastructure relay is not available. The coverage probability and spectral efficiency of relay-assisted mmWave cellular networks are derived when the D2D links are implemented in either uplink mmWave or uplink microwave bands. Deng *et al.* [25] proposed a low-complexity architecture design technique for relay-assisted mmWave communication systems to reduce the number of RF chains while mitigating the effect of residual loopback self-interference.

Another important matter in relay-assisted mmWave networks is to find an optimal location for the fixed or mobile RS [26]–[28]. Sakarellos *et al.* [26] investigated the optimal placement of radio fixed relays in mmWave dual-hop networks when different types of relays are employed. Kong *et al.* [27] proposed a new method (AutoRelay) for autonomous mobile relays, such as drones and self-driving cars, to determine the optimal position accurately and quickly. Sanchez and Alonso [28] proposed a two-hop relay architecture using mobile relay technology for high-speed trains with long-term evolution (LTE) and mmWave bands.

Thus, RS deployment can be a possible solution for the blockage problem in mmWave cellular systems. However, to the best of our knowledge, studies on the design of a training sequence that allows an MS to find an optimal RS in relay-assisted mmWave cellular systems have not yet been reported. The first problem to be considered when designing a training sequence is the number of possible IDs to be generated in a relay-assisted mmWave cellular system. In this system, the BS/RS should forward data to an adjacent RS/BS with an LoS link to the MS whenever a blockage occurs between the BS/RS and MS. Then, the adjacent RS/BS forwards the data to the MS. Implementation of this concept would require the MS to monitor the channel conditions of adjacent RSs/BSs in case the blockage occurs on the serving link. This would require the RSs and BSs to periodically transmit training signals with their node IDs by sweeping their transmitter (Tx) beams. The source of the serving link could be either a BS or RS. Because the MS needs to find the channel conditions of adjacent RSs (or BSs) in a multicell environment, the training signals transmitted from the RSs and BSs would have to contain information on their identity (ID) (Cell ID and RS ID), unlike traditional cellular systems where repeaters/relays do not have their ID. In relay-assisted mmWave cellular systems, the MS would need to receive the data through the optimal (aligned) beam of the selected RS, unlike a traditional cellular system. The training sequence would have to provide a large number of different sequences because the number of required training sequences increases proportionally to the multiplication of the number of cells (BSs) and the number of RSs in a cell. In 5G NR, there are 1,008 different physical cell identities (PCIs) [9], [10]. Accordingly, the training signal should have the capability to generate a large number of IDs and have a low correlation to enable MSs to distinguish different sequences in multi-cell multi-relay environments.

The training sequence in a relay-assisted mmWave cellular system based on OFDM can be transmitted in either preamble or pilot format. In the preamble format, only a training sequence is transmitted as in synchronization signal block (SSB) in 5G NR [9]. However, in relay-assisted mmWave cellular systems, blockage on the serving link may occur anytime. Thus, the pilot format would be more effective, because the MS would need to monitor the channel conditions of adjacent RSs/BSs while data transmission takes place in the serving link. In addition, the processing time for RS selection and beam alignment would be shorter when the pilot format is used, because channel monitoring can be performed using pilots in OFDM symbols. If the preamble format were to be used, the processing time would be much longer because the period between preambles (SSBs) is much longer compared with the OFDM symbol period [10]. For example, if the link reestablishment is performed using the

preamble (SSB) defined in 3GPP specifications, the processing time will be several hundred milliseconds. Note that the processing time is proportional to the preamble period and the preamble period ranges from 5ms to 160ms depending on channel condition. However, in untethered virtual reality (VR), excessive latency more than 15ms can cause motion sickness [6]. The time delay, 15ms, is much shorter than the time required for link re-establishment in the preamble-based approach.

However, the use of the pilot format would cause the pilot signals received from adjacent RSs (or BSs) to experience different symbol time offset (STO) due to the different distances. Although the same subcarriers would be assigned to the pilots for all RSs (or BSs) to reduce interference in the data subcarriers, different STO may generate significant inter-symbol interference (ISI). Because the MS would have to distinguish the sequences from the pilots, we need to consider a method to overcome the ISI problem caused by multiple RSs with different STOs, in addition to the well-known ISI problem caused by a multipath channel [30].

Our approach to address these problems starts with the design of a frame structure, which enables an MS to monitor the channel condition using the pilot signals received from adjacent RSs (or BSs) in a relay-assisted mmWave cellular system. Next, we develop a method to overcome the ISI problem caused by pilots from multiple RSs in different locations. This leads us to propose two different types of pilot sequences, which can generate a large number of IDs: PS1 and PS2. Here, PS1 and PS2 are pilot signals based on the Zadoff-Chu (ZC) sequence and m-sequence, respectively [31]. The correlation property of PS2 is derived and compared with that of PS1 and the Gold sequence (GS). Simulations are performed to verify the properties, constraints, advantages, and disadvantages of the sequences.

The remainder of this paper is organized as follows. Section II describes a system model for RS-assisted mmWave cellular systems. The operational concept, frame structure, and synchronization problems for pilot-based RS-assisted mmWave cellular systems are discussed. Section III describes the two different types of sequence (PS1 and PS2) for RS-assisted mmWave cellular systems. The correlation property of PS2 is also derived and compared with that of PS1 and GS. Section IV presents an evaluation of the performance of the proposed pilot sequence using a simple model of a pilot-based mmWave cellular system with a one-hop relay. Conclusions are drawn in Section V.

II. SYSTEM MODEL

MmWave signals are highly sensitive to blockage effects compared with low-frequency radio frequency (RF) signals. The blockage can be caused by relatively static obstacles such as buildings and mountainous terrain, or by mobile users such as walking people and vehicles [1], [2]. Two blockage models were proposed by the 3GPP study group on mmWave channel models [6].

Model A, which represents a stochastic-based model, and Model B, a model based on the channel and spatial properties, respectively [32], [33]. In this study, we used Model B for blockage modeling and simulation because it is geometric-based and easier to control the number of blockers and their distances.

Fig. 1 illustrates the operational concept of a pilot-based RS-assisted mmWave cellular system. The figure shows one BS and one RS for simplicity. It is assumed that a dedicated link is established between the BS and RS through wireless or wired backhaul. Although only one BS and one RS are shown, the concept could easily be extended to multi-cell multi-relay environments. In Phase 1, an LoS link is assumed to exist between the BS and MS, and the MS is served by the BS. The RS is sweeping its transmit (Tx) beam to transmit pilot signals in case the blockage occurs between the BS and MS. In this phase, the BS and RS play the roles of serving source and beam sweeping source, respectively. The serving source transmits data and pilot signals simultaneously whereas the beam-sweeping source transmits only pilot signals for possible blockage. As shown in the figure, the pilot signals in the serving source and all beam-sweeping sources are allocated on the same subcarriers to avoid interference between the data and pilots. In Phase 2, blockage occurs on the serving link between the BS and MS. Then, the MS starts receive (Rx) beam sweeping to find an optimal RS and corresponding Tx/Rx beams using the pilot signals received from adjacent RSs/BSs. Comparing the signals received from adjacent BSs/RSs, the MS selects the link with a highest power. In Phase 3, the MS receives data from the selected RS with the corresponding Tx/Rx beam. In this phase, the RS and BS play the roles of serving source and beam-sweeping source, respectively. In Phase 4, the blockage occurs on the serving link between the RS and MS. The MS starts Rx beam sweeping to find an optimal serving source (BS/RS) and corresponding Tx/Rx beam. If the BS is selected as an optimal node with the corresponding Tx/Rx beam, it returns to the scenario in Phase 1.

Fig. 2 illustrates the structure of the framework of the pilot-based RS-assisted mmWave cellular system depicted in Fig. 1. In this figure, the system is assumed to be operated in time division duplexing (TDD) mode with one RF chain for all nodes (BS, RS, MS). The first and second frames (rows) show the signals transmitted from BS to MS and from RS to MS, respectively. The third and fourth frames (rows) show detailed versions of the first and second frames (rows). In the first slot, the BS and RS have the roles of serving source and beam sweeping source, respectively. In the second slot, the roles of the RS and BS are exchanged. The serving beam period and beam-sweeping period take place exclusively and alternately in time. The serving beam period is composed of multiple downlink (DL) and uplink (UL) data transmission periods. The beam-sweeping period is composed of multiple pilot transmission periods and link setup periods. During the pilot transmission period, the beam-sweeping sources transmit their pilot signals in different beam directions. In the link

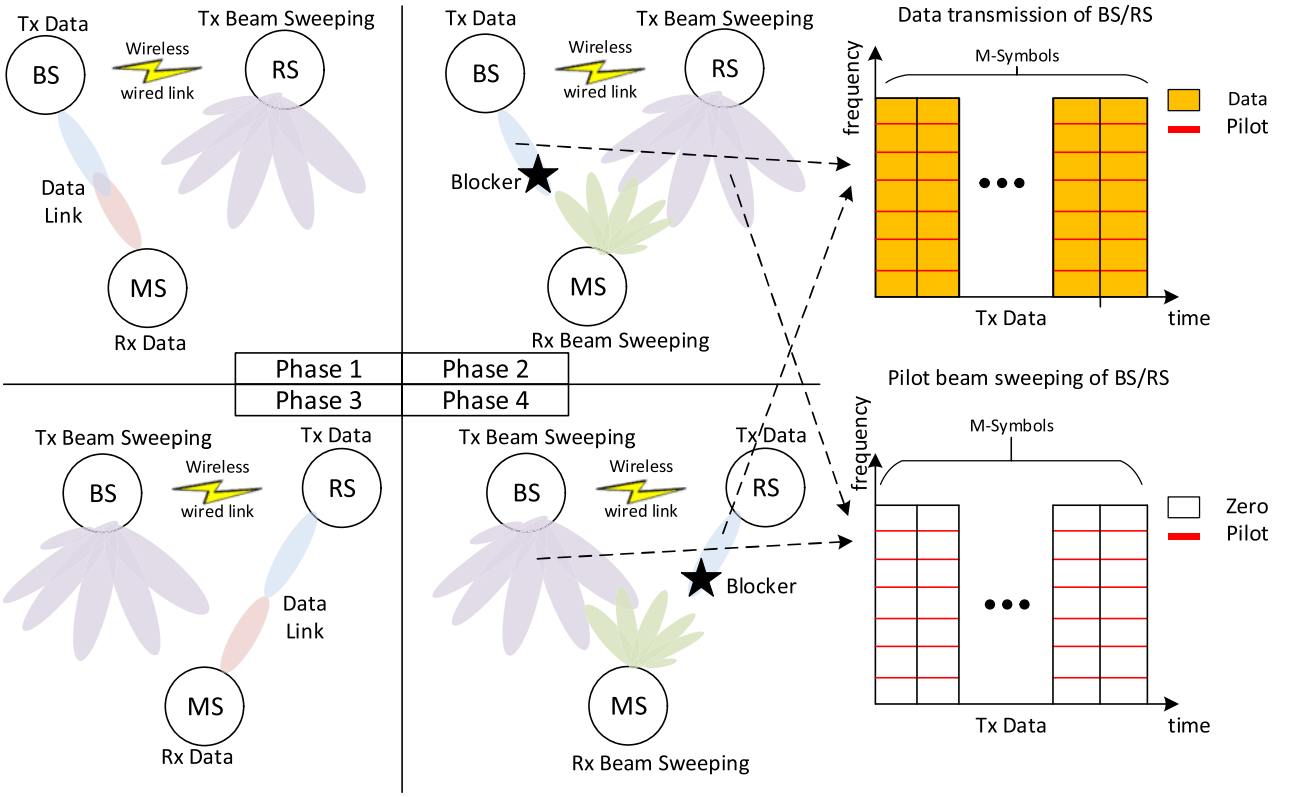

FIGURE 1. Concept of an RS-assisted mmWave communication system.

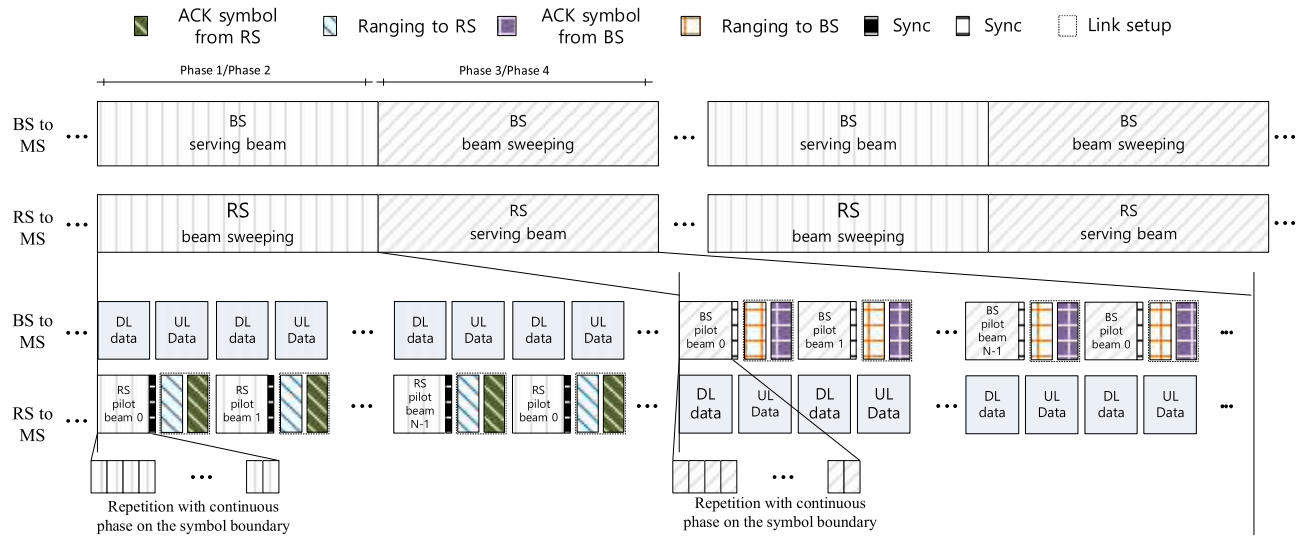

FIGURE 2. Structure of the proposed framework for the pilot-based RS-assisted mmWave cellular system.

setup period, the MS and beam-sweeping sources set up the connection based on the measurement result. The link setup period is composed of a ranging/request signal from MS and response/ACK signal from RS/BS.

While the MS receives data from the serving source (before blockage occurs), the MS is synchronized to this source. The MS not only receives pilot signals from the serving source but also from adjacent RSs/BSs for channel monitoring while it receives data from the serving source. However, because the MS is synchronized to the serving source, the pilot signals received from adjacent beam-sweeping sources are not synchronized to the MS. The pilot signals experience different STOs because of the different locations of the RSs/BSs. Thus, discontinuities may occur in the pilot signals received from beam-sweeping sources during the fast Fourier transform (FFT) window, which causes ISI. The ISI may degrade the

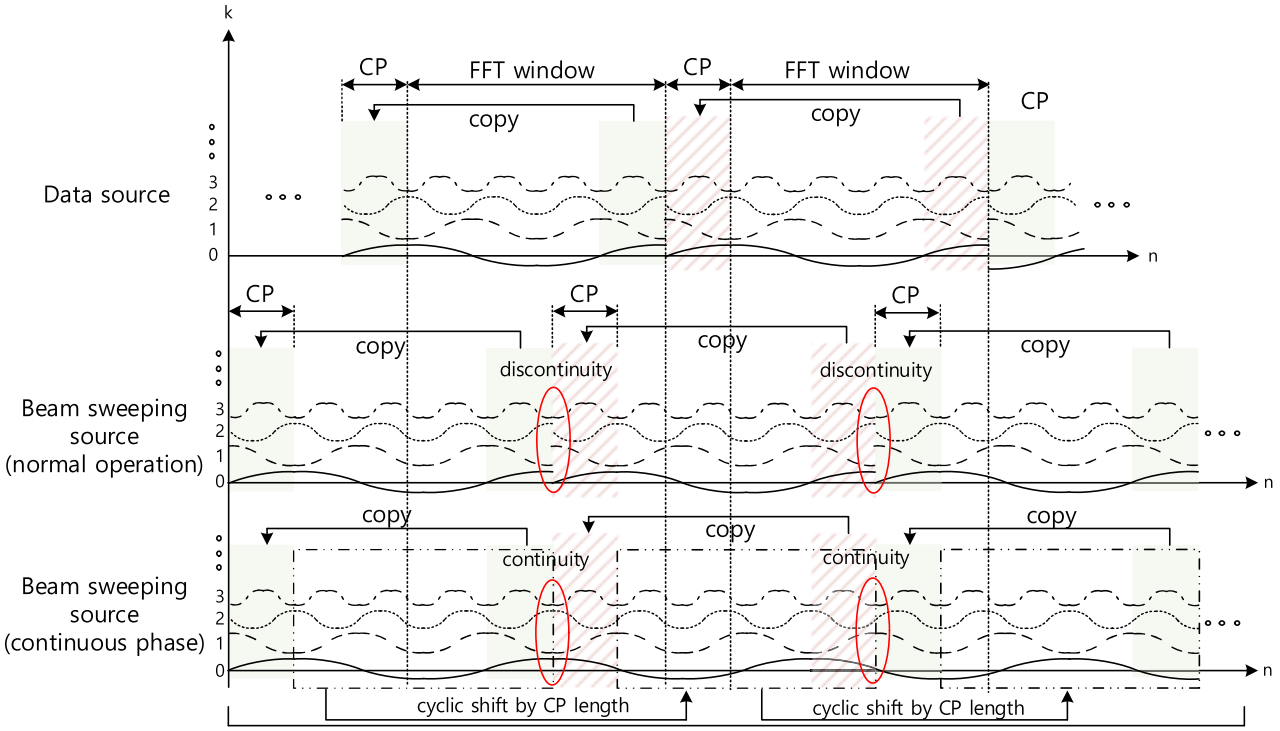

FIGURE 3. Concept of pilot signal transmission with continuous phase.

performance of optimal node selection with the corresponding Tx/Rx beam, because the MS is synchronized to the serving source. To avoid this problem, the MS can perform node selection after synchronizing to all adjacent beam-sweeping sources. However, the synchronization process is computationally intensive and requires a significant amount of operational time.

This study proposes a simple yet effective method for pilot-based RS-assisted mmWave cellular systems to circumvent the synchronization problem that arises during channel monitoring for beam-sweeping sources. The discontinuity within the FFT window of the MS, synchronized to the serving source, is caused by a discontinuous phase on the symbol boundary and the STOs among the received pilot signals. The STO effect cannot be easily compensated in a real environment because of different propagation delays from different beam-sweeping sources. To solve the synchronization problem, two different concepts are used when designing the frame structure and pilot signal. First, each beam sweeping source maintains its Tx beam direction during the sub-period of DL data transmission in the serving source such that the discontinuity caused by beam switching in beam-sweeping sources can be avoided during the sub-period of DL data transmission. As illustrated in Fig. 2, the RS/BS pilot beams are maintained during the sub-period of BS/RS DL data transmission. The MS performs Rx beam switching while the beam-sweeping source maintains its Tx beam direction. Second, the pilot signals in beam-sweeping sources are designed to have a continuous phase on the symbol boundary during the sub-period of DL data transmission. The cyclic prefix (CP) is normally used to avoid the ISI problem caused by a multipath channel [30]. However, even with the CP, a discontinuous phase may occur on the boundary of an OFDM symbol in a pilot-based RS-assisted mmWave cellular system. The continuous phase can be obtained by a cyclic shift of the OFDM symbol by the amount corresponding to the CP length. Then, although STOs exist in the pilot signals received from the beam-sweeping sources, the discontinuity does not appear within the FFT window of MS. Fig. 3 depicts an example of time-domain pilot signals received from adjacent beam-sweeping sources with different STOs, when the MS is synchronized to the serving source. In a normal mode, discontinuities can be observed within the FFT discontinuity does not occur. If the system were to be operated in the normal mode, the orthogonality among the subcarrier frequency components would also be destroyed, resulting in inter-channel interference (ICI). The performance of DL data transmission can be significantly degraded by the effect of ICI. The proposed method can reduce the effect of ICI as well as ISI in pilot-based RS-assisted mmWave cellular systems.

Fig. 4 depicts the signal-to-interference ratio (SIR) on DL data subcarriers when the value of STO varies. Here, the FFT size, pilot spacing, and CP length are set to 4096, 32, and 288, respectively. The figure shows that, in the normal mode (discontinuous phase), the SIR decreases significantly

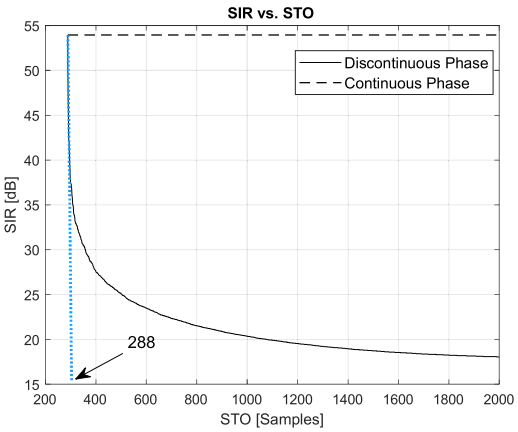

FIGURE 4. Signal to interference ratio (SIR) vs. symbol timing offset (STO).

as the STO increases, due to the ICI effect. However, the SIR remains unchanged when the proposed method (continuous phase) is used.

Next, a system model for the proposed pilot-based mmWave is described. As shown in Fig. 2, the frame consists of a data transmission period, pilot transmission period, and link setup period. In this study, we focus only on the pilot transmission period because various conventional techniques can be used in the other periods.

In the pilot transmission period, the pilot signal on the k-th subcarrier of the beam-sweeping source in an OFDM system is given by

$$[\mathbf{x}_b^{c,q}]_k = X_{b,k}^{c,q} = \begin{cases} [\mathbf{s}^{c,q}]_{v_{k_P}}, & k \in \{k_P\} \\ 0, & \text{otherwise} \end{cases} \tag{1}$$

where $0 \le k < N_F, 0 \le v_{k_P} < N, 0 \le b < N_B, 0 \le q < N_N$ and $0 \le c < N_C$. Here, $k, k_P, v_k, \{k_P\}, N, b, N_B, q, N_N$, and N_F are the subcarrier index, pilot subcarrier index, pilot sequence index corresponding to k_P, pilot subcarrier set, sequence length, beam ID (BID), number of BIDs, node ID (NID), number of NIDs, and FFT size, respectively. Furthermore, c and N_C are cell ID (CID) and number of CIDs, respectively. $[\mathbf{s}]_n$ denotes the n-th element of pilot sequence vector $\mathbf{s}$. The pilot signal of the serving source can be also given by (1) except that other subcarriers are used for data. In this study, it is assumed that there exist multiple BSs (cells) and multiple RSs in a cell. The RSs in the same cell have the same CID but different NIDs. NID 0 is allocated to the BS. Thus, the node can be either an RS or BS. The signal received by the i-th Rx beam from the beam-sweeping source and serving source is given in (2) on the bottom of this page.

In (2), h, l, and L_h denote the channel coefficient, channel tap index, and the number of taps, respectively, and the superscript s denotes the serving source. η_{Tx} and η_{Rx} denote Tx and Rx beam-forming gain, respectively. In addition, $\sigma^{c,q}$, σ_S, and W denote the STO of the beam-sweeping source, STO of the serving source, and noise, respectively. In the RS beam-sweeping period, the signal in (2) is given by the pilot signals received from the beam-sweeping sources ($q \ge 1$) and serving source (BS: $q = 0$). In the BS beam-sweeping period, the MS is served by the RS. In this period, only BSs are considered as potential beam-sweeping sources because this study is only concerned with one-hop relays.

To select a target node, the MS performs correlation between the received signal and pilot sequence as follows:

$$R_{i,b,m}^{c,q} = |\sum_{k=0}^{N_F-1} Y_{i,b,k}(X_{b,k}^{c,r})^* e^{j2\pi mk/N_F}|^2 \tag{3}$$

$$R_{i,b}^{c,q} = \max\{R_{i,b,m}^{c,q}\}, \tag{4}$$

where the term $e^{j2\pi mk/N_F}$ is multiplied to compensate for the effect of STO in the frequency domain. When the MS is synchronized to the serving source, the STO value m, estimated by the conventional synchronization technique, approximates σ_S. When the received signal is multiplied by this term,

$$Y_{i,b,k} = \begin{cases} \underbrace{\sum_{c=0}^{N_C}\sum_{q=1}^{N_N-1}\sum_{l=0}^{L_h-1} h_{b,l,k}^{c,q}\eta_{Rx,i}\eta_{Tx,b}^{c,q}X_{b,k}^{c,q}e^{-j2\pi\sigma^{c,q}k/N}}_{\text{Pilot signals received from beam sweeping sources (RS)}} \\ \quad + \underbrace{\sum_{l=0}^{L_h-1} h_{b,l,k}^{s}\eta_{Rx,i}^{s}\eta_{Tx,b}^{s}X_{b,k}^{s}e^{-j2\pi\sigma_S k/N}}_{\text{Pilot signal received from serving source (BS)}} + W_{i,b,k} & \text{RS beam sweeping period} \\ \underbrace{\sum_{c=0}^{N_C}\sum_{l=0}^{L_h-1} h_{b,l,k}^{c,0}\eta_{Rx,i}\eta_{Tx,b}^{c,0}X_{b,k}^{c,0}e^{-j2\pi\sigma^{c,0}k/N}}_{\text{Pilot signals received from beam sweeping sources (BS)}} \\ \quad + \underbrace{\sum_{l=0}^{L_h-1} h_{b,l,k}^{s}\eta_{Rx,i}\eta_{Tx,b}^{s}X_{b_D,k}^{s}e^{-j2\pi\sigma_S k/N}}_{\text{Pilot signal received from serving source (RS)}} + W_{i,b,k} & \text{BS beam sweeping period} \end{cases} \tag{2}$$

the STO effect caused by the serving source is compensated for. However, the STOs caused by beam sweeping sources generate discontinuous phases within the FFT window of the MS unless the proposed compensation method is used. Finally, the target node can be selected by determining the parameters that maximize the correlation function as follows:

$$\{\hat{c}, \hat{q}, \hat{b}, \hat{i}\} = \arg \max_{c,q,b,i} \{R_{i,b}^{c,q}\}, \tag{5}$$

where $\hat{c}$, $\hat{q}$, $\hat{b}$, and $\hat{i}$ denote the estimated CID, NID, BID, and Rx beam index, respectively. Because the BID and Rx beam index can easily be identified by the transmission time as in 5G NR, we develop a pilot design technique which enables us to estimate the CID and NID in a multi-cell multi-relay environment. This technique is discussed in Section III

III. THE PROPOSED PILOT SEQUENCES FOR RS-ASSISTED mmWave CELLULAR SYSTEMS

In this section, we describe two different types of pilot sequences, PS1 and PS2, for an OFDM-based mmWave cellular system with one-hop relays. Specifically, PS1 and PS2 are pilot signals based on the ZC sequence and m-sequence, respectively. Both of these sequences are widely used for preamble and pilot design owing to their low correlation property. PS1 is generated by allocating CID and NID to the parameters of the ZC sequence to provide a large number of IDs. PS2 can be considered a new sequence based on the m-sequence to provide a large number of IDs with low cross-correlation.

PS1 is generated by mapping CID and NID to a root index and cyclic shift of a prime-length ZC sequence, respectively, as follows:

$$\begin{aligned}[\mathbf{s}^{c,q}]_v &= e^{-j\pi(\tilde{r}_c(qG)^2+qG)/N} e^{-j\pi r_c v(v+1)/N} e^{-j2\pi r_c G v/N} \\ &= e^{-j\pi r_c(v+\tilde{r}_c qG)(v+\tilde{r}_c qG+1)/N} = Z^{r_c}_{v+\tilde{r}_c qG}\end{aligned} \tag{6}$$

Here, $0 < r_c < N, 0 \le v < N$, and $0 \le q \le \lfloor N/G \rfloor$. Z, r_c, and $\tilde{r}_c$ are the ZC sequence, root index of the ZC sequence corresponding to CID c, and modulo inverse of r_c, respectively. G is the parameter for phase rotation to distinguish sequences among different NID q. Other parameters are defined in (1). The pilot sequence vector $\mathbf{s}$ in (6) is allocated to the subcarriers as given in (1). The phase rotation with a slope qG is converted into the cyclic shift with a spacing $\tilde{r}_c qG$ because of the property of the ZC sequence. In PS1, N_C and N_N become $N-1$ and $\lfloor N/G \rfloor$, because CID and NID are distinguished by the root index and cyc46lic shift, respectively. However, because the STO has the effect of a linear phase rotation in the frequency domain, the STO can produce an ambiguity in NID detection. To avoid this situation, it is necessary to specify the parameter G such that its value is sufficiently large to cover the phase rotation caused by STO. When $G = 1$, N_N is equal to $N-1$. However, N_N decreases when G increases. The cross-correlation value of PS1 becomes zero if two nodes are in the same cell (different NIDs, same CID), and $1/\sqrt{N}$ if two nodes are in different cells (different CIDs) regardless of their NIDs.

The m-sequence has been widely used for preamble and pilot design owing to its good auto-correlation property. However, it has limited ability to distinguish different sequences because of its poor cross-correlation property. The GS is often used for applications in multiple-access communication systems because it can provide a large set of sequences with enhanced cross-correlation properties. The GS is obtained by selecting preferred pairs of m-sequences and their combinations. Unlike the m-sequence (two-valued), the cross-correlation function of GS is three-valued. PS2 is proposed to reduce the cross-correlation value further while maintaining a large set of sequences.

PS2 is generated by multiplying two sequences, obtained by the DFT of one m-sequence, with different cyclic shifts as follows:

$$[\mathbf{s}^{c,q}]_v = P_v^{d_0^{c,q}, d_1^{c,q}} = P_{v+d_0^{c,q}} (P_{v+d_1^{c,q}})^*, \tag{7}$$

where $N = 2^n - 1$, $P_v = (1/N)^{1/2} \sum_{n=0}^{N-1} p_n e^{-j2\pi vn/N}$, $0 \le d_0^{c,q}, \ d_1^{c,q} < N$, and $d_0^{c,q} \ne d_1^{c,q}$.

Here, p and P are the m-sequence and the DFT of the m-sequence, respectively. The pilot sequence vector $\mathbf{s}$ in (7) is allocated to the subcarriers as given in (1). Different values of cyclic shifts (d_0, d_1) are assigned to P, depending on the values of CID and NID (c, q). Because PS2 is obtained by the multiplication of two different P and P^*(DFTs of the m-sequence) with different cyclic shifts, it is not affected by the ambiguity problem in CID and NID detection. Because any values of (d_0, d_1) can be used as long as $d_0 \ne d_1$, the number of available sequences in PS2 becomes $(N-1)N$. The number of NIDs (N_N) mapped to each CID becomes $\lfloor (N-1)N/N_C \rfloor$.

Next, the correlation property of PS2 is analyzed. The correlation function of PS2 is defined as

$$|C_{d_2^{c,q}, d_3^{c,q}}^{d_0^{c,q}, d_1^{c,q}}| = |\sum_{v=0}^{N-1} P_v^{d_0^{c,q}, d_1^{c,q}} (P_v^{d_2^{c,q}, d_3^{c,q}})^*|. \tag{8}$$

Ignoring c and q for notational convenience, the correlation function of PS2 can be re-written as

$$\begin{aligned}C_{d_2,d_3}^{d_0,d_1} = \frac{1}{N} \sum_{v=0}^{N-1} \sum_{n_0=0}^{N-1} \sum_{n_1=0}^{N-1} \\ \times \begin{pmatrix} p_{n_0} e^{-j2\pi n_0(v+d_0)/N} p_{n_1} e^{j2\pi n_1(v+d_1)/N} \\ \times (P_{v+d_2})^* P_{v+d_3} \end{pmatrix}\end{aligned} \tag{9}$$

If n_1 and n_3 are replaced with $n_1 = n_0 + \delta_0$ and $n_3 = n_2 + \delta_1$, respectively, (9) can be expressed as

$$\begin{aligned}C_{d_2,d_3}^{d_0,d_1} = \frac{1}{N} \sum_{\delta_0=1}^{N-1} \sum_{n_0=0}^{N-1} p_{n_0} p_{n_0+\delta_0} e^{-j2\pi n_0(d_0-d_1)/N} e^{j2\pi \delta_0 d_1/N} \\ \times \sum_{v=0}^{N-1} (P_{v+d_2})^* P_{v+d_3} e^{j2\pi \delta_0 v/N},\end{aligned} \tag{10}$$

where

$$\Gamma = \sum_{n_0=0}^{N-1} p_{n_0} p_{n_0+\delta_0} e^{-j2\pi n_0(d_0-d_1)/N} e^{j2\pi\delta_0 d_1/N}$$

$$\Omega = \frac{1}{N}\sum_{\delta_0=1}^{N-1}\sum_{n_0=0}^{N-1} p_{n_0} p_{n_0+\delta_0} e^{-j2\pi n_0(d_0-d_1)/N} e^{j2\pi\delta_0 d_1/N}$$

$$\Upsilon = \sum_{v=0}^{N-1} (P_{v+d_2})^* P_{v+d_3} e^{j2\pi\delta_0 v/N}.$$

Here, the case with $\delta_0 = 0$ is removed, because Γ is 0 when δ_0 is 0. The use of the "shift-and-add property" of the m-sequence [34] enables us to replace the term $p_{n_0}p_{n_0+\delta}$in Ω by $p_{n_0+D_\delta}$.

Note that the "shift-and-add property" states that multiplication of an m-sequence and its own cyclic shift is another m-sequence. Here, D_δ denotes the amount of shift caused by multiplying an m-sequence by its shifted version with an offset δ ranging from 1 to $N-1$. For all shifts (δ), there exists a unique integer D_δ such that the relationship holds. Then, Ω in (10) can be expressed as

$$\Omega = \sqrt{N} P_{(d_0-d_1)} \sum_{\delta_0=1}^{N-1} e^{j2\pi\delta_0 d_1/N} e^{j2\pi D_{\delta_0}(d_0-d_1)/N}. \quad (11)$$

Furthermore, Υ in (10) can be re-written as

$$\Upsilon = \sum_{v=0}^{N-1}\sum_{n_2=0}^{N-1}\sum_{n_3=0}^{N-1} \left(\begin{matrix} p_{n_2} p_{n_3} e^{j2\pi n_2 d_2/N} e^{-j2\pi n_3 d_3/N} \\ \times e^{j2\pi\delta_0 v/N} e^{j2\pi(n_2-n_3)v/N} \end{matrix} \right). \quad (12)$$

If n_3 is replaced with $n_3 = n_2 + \delta_1$, (12) can be expressed as

$$\Upsilon = \left(\begin{matrix} \sum_{\delta_1=1}^{N-1}\sum_{n_2=0}^{N-1} p_{n_2} p_{n_2+\delta_1} e^{j2\pi n_2(d_2-d_3)/N} e^{-j2\pi\delta_1 d_3/N} \\ \times \sum_{v=0}^{N-1} e^{j2\pi\delta_0 v/N} e^{-j2\pi\delta_1 v/N} \end{matrix} \right)$$

$$= \sqrt{N} P_{(d_3-d_2)} \left(\begin{matrix} \sum_{\delta_1=1}^{N-1} e^{-j2\pi\delta_1 d_3/N} e^{j2\pi D_{\delta_1}(d_3-d_2)/N} \\ \times \sum_{v=0}^{N-1} e^{j2\pi\delta_0 v/N} e^{-j2\pi\delta_1 v/N} \end{matrix} \right) \quad (13)$$

Substituting (11) and (13) into (10), it can be re-written as

$$C_{d_2,d_3}^{d_0,d_1} = \frac{1}{N}\Omega\Upsilon = P_{(d_0-d_1)} P_{(d_3-d_2)} \underbrace{\sum_{\delta_0=1}^{N-1} e^{j2\pi D_{\delta_0} a/N} e^{-j2\pi\delta_0 b/N}}_{A} \quad (14)$$

where $a = (d_0 - d_1 + d_3 - d_2)$ and $b = (d_3 - d_1)$. When both a and b are zero, $|A|$ becomes $N-1$. However, when a is not equal to b, $|A|^2$ in (14) can be expressed as

$$|A|^2 = \sum_{\delta_0=1}^{N-1}\sum_{\bar{\delta}_0=1}^{N-1} e^{j2\pi(D_{\delta_0}-D_{\bar{\delta}_0})a/N} e^{-j2\pi(\delta_0-\bar{\delta}_0)b/N}$$
$$= \sum_{\delta_0=1}^{N-1}\{1 + \sum_{\bar{\delta}_0=1,\bar{\delta}_0\neq\delta_0}^{N-1} e^{j2\pi(D_{\delta_0}-D_{\bar{\delta}_0})a/N} e^{-j2\pi(\delta_0-\bar{\delta}_0)b/N}\}. \quad (15)$$

When $(\bar{\delta}_0 - \delta_0)_{\%N}$ is equal to τ ranging from 1 to $N-1$, (15) is expressed as (16), shown at the bottom of this page. Here, % represents the modulo operation. Note that $N-\tau$ is not considered for the value of δ_0 because $D_{(\delta_0+\tau)_{\%N}}$ becomes D_0 (out of range). For notational convenience, $D_{\delta_0+\tau}$ is used for $D_{(\delta_0+\tau)_{\%N}}$ in the following equations. To simplify Ψ in (16) further, the following proposition and corollaries are made.

[Proposition 1]: When τ is a constant integer ranging from 1 to $N-1$, $(D_\delta - D_{\delta+\tau})_{\%N}$, for a different value of δ must have a different value ranging from 1 to $N-1$ except $N-\tau$.

Proof) See Appendix A

[Corollary 1]: $(D_\delta - D_{-\delta})_{\%N}$ is δ.

Proof) See Appendix B

[Corollary 2]: When τ is a constant integer ranging from 1 to $N-1$, $(D_\delta - D_{\delta+\tau})_{\%N_S}$, cannot be 0 or $N-\tau$ if δ has a value ranging from 1 to $N-1$ except $N-\tau$.

Proof) See Appendix C

Because the variable δ_0 in Ψ of (16) ranges from 1 to $N-1$, the range of D_{δ_0} is from 1 to $N-1$. Furthermore, because τ is a constant integer ranging from 1 to $N-1$, the range of $(D_{\delta_0} - D_{\delta_0+\tau})_{\%N}$ is from 1 to $N-1$. According to Proposition 1, $(D_\delta - D_{\delta+\tau})_{\%N}$ has a different value for a different δ_0. Note that the value $N-\tau$ is excluded from the range of δ_0 in the summation term of Ψ, and $(D_\delta - D_{\delta+\tau})_{\%N}$ cannot be $N-\tau$ (Corollary 2). Thus, the range of $(D_\delta - D_{\delta+\tau})_{\%N}$ is from 1 to $N-1$ except $N-\tau$. If $(D_\delta - D_{\delta+\tau})_{\%N}$ is replaced

$$|A|^2 = \begin{cases} N-1+(N-2)\sum_{\tau=1}^{N-1} e^{j2\pi\tau b/N} = 1, & a=0\,\&\,a\neq b \\ N-1+\sum_{\tau=1}^{N-1} e^{j2\pi\tau b/N}\underbrace{\{\sum_{\delta_0=1,\delta_0\neq N-\tau}^{N-1} e^{j2\pi(D_{\delta_0}-D_{(\delta_0+\tau)_{\%N}})a/N}\}}_{\Psi} & a\neq 0\,\&\,a\neq b \end{cases} \quad (16)$$

by $\tilde{D}_\delta$, Ψ can be re-written as

$$\Psi = \sum_{\tilde{D}=1,\tilde{D}\neq N-\tau}^{N-1} e^{j2\pi\tilde{D}a/N} = \sum_{\tilde{D}=0}^{N-1} e^{j2\pi\tilde{D}a/N} - e^{j2\pi 0a/N} - e^{j2\pi(N-\tau)a/N}. \quad (17)$$

The first term on the right-hand side becomes zero because a is an integer number. The second term becomes one. The third term can be expressed by $e^{j2\pi(N)a/N}e^{j2\pi(-\tau)a/N}$ where the first term becomes one for any integer value of a. Thus, Ψ in (23) can be simplified as

$$\Psi = -1 - e^{-j2\pi\tau a/N}. \quad (18)$$

Then, using (23), $|A|^2$ in (16) is given by

$$|A|^2 = \begin{cases} (N-1)^2, & a = 0 \& b = 0 \\ N+1, & a \neq 0 \& b \neq 0 \& a \neq b \\ 1, & \text{otherwise} \end{cases} \quad (19)$$

Using (10) and (24), the correlation property of PS2 is given by

$$|C_{d_2,d_3}^{d_0,d_1}| = |\sum_{v=0}^{N-1} P_v^{d_0,d_1}(P_v^{d_2,d_3})^*| \quad (20)$$

$$|C_{d_2,d_3}^{d_0,d_1}| == \begin{cases} ((N)^2-1)/N, & a = 0 \& b = 0 \\ (N+1)^{3/2}/N, & a \neq 0 \& b \neq 0 \& a \neq b \\ (N+1)/N, & \text{otherwise} \end{cases} \quad (21)$$

Here, the first condition, "$a = 0$ & $b = 0$," corresponds to the case of the same (d_0, d_1) and (d_2, d_3), i.e., the same pilot sequences. The correlation between the same pilot sequence of PS2 becomes $((N)^2-1)/N$. The second condition, "$a \neq 0 \& b \neq 0 \& a \neq b$," occurs when d_0 and d_1 are different from d_2 and d_3, respectively, and b is different from $d_2 - d_0$. The maximum cross-correlation of PS2 occurs when the pilot sequences have different (d_0, d_1) and (d_2, d_3), and is given by $(N+1)^{3/2}/N$. Otherwise, the cross-correlation of PS2 becomes $(N+1)/N$. Fig. 5, which shows an example of the correlation function of PS2 when $N = 63$, compares the analytical solution in (21) and the simulation result as a function of the sequence index (condition). As can be seen in (21), the correlation function of PS2 is three-valued.

The first condition corresponds to the case of the same pilot sequences. In this case (auto-correlation), a peak occurs at the sequence index and its value becomes one after normalization with the maximum value. In PS2, the maximum cross-correlation value (0.1289) is obtained when the second condition is satisfied. A small cross-correlation value (0.01612) is obtained when the third condition is satisfied. Because the analytical solution and simulation result are almost identical, the lines in the figure are indistinguishable.

Fig. 6 compares the correlation functions of PS1, P2, and GS for $N = 63$ and $N = 127$. Here, a cumulative distribution function (CDF) is used to compare the distribution of

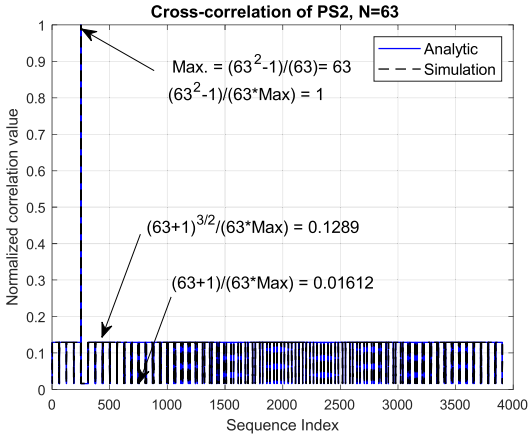

FIGURE 5. Correlation property of PS2.

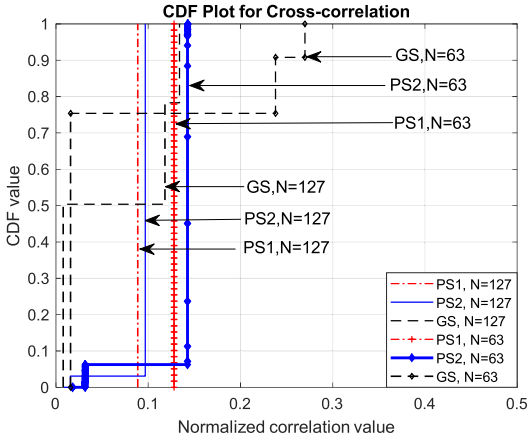

FIGURE 6. Correlation properties of PS1, PS2, and GS.

correlation values for all possible sequence indices. As can be seen in this figure, the maximum correlation value of PS2, $(N+1)^{3/2}/N$, is smaller than the maximum cross-correlation value of GS, $(2^{\lfloor(\log_2(N+1)+2)/2\rfloor}+1)$, and slightly larger than the maximum correlation value of PS1, $1/\sqrt{N}$.

These results are summarized in Table 1, which indicates that the analytical and simulation results are almost identical for all three sequences (PS1, PS2, and GS). The maximum correlation values of PS1 and PS2 are significantly smaller than that of GS when the same number of sequence lengths is used. In terms of the number of available sequences, PS2 and GS can provide $(N-1)N$ and $(N+1)N$ different sequences, respectively.

PS2 can generate a slightly smaller number of sequences than GS. However, the number of available sequences in PS2 and GS become similar as the sequence length N increases. On the other hand, the number of available sequences in PS1 is significantly smaller than that of PS2 because of the ambiguity problem in NID detection. However, PS2 does not experience the ambiguity problem when STOs are present. Moreover, GS cannot have sequence lengths with a degree (primitive polynomial) equal to multiples of 4, whereas there is no restriction on the length

TABLE 1. Maximum correlation values of PS1, PS2, and GS with different sequence lengths.

	Maximum Correlation	N=31 Analytic / Simulation	N=63 Analytic / Simulation	N=127 Analytic / Simulation
PS1	$1/\sqrt{N}$	0.1796 / 0.1796	0.1280 / 0.1280	0.0887 / 0.0887
PS2	$(N+1)^{3/2}/N$	0.1886 / 0.1885	0.1289 / 0.1290	0.0897 / 0.0897
GS	$(2^{\lfloor(\log_2(N+1)+2)/2\rfloor}+1)$	0.2903 / 0.2903	0.2698 / 0.2698	0.1339 / 0.1339

TABLE 2. Simulation parameters.

Channel model	Spatial Channel Model (SCM)
K-factor	15 dB
Pathloss model	UMi
Blockage model	Model B
Carrier frequency	28 GHz
Subcarrier spacing	120 kHz
FFT size	4096
Length of pilot sequence	127
Antenna elements in Tx (URA)	16
Antenna elements in Rx (ULA)	8

of PS1 and PS2. Thus, PS2 is suitable for relay-assisted cellular systems, which require a large number of IDs and low cross-correlation.

IV. SIMULATIONS

The performance of the proposed pilot sequence is evaluated using a simple model of a pilot-based mmWave cellular system with a one-hop relay. The 5G NR specification is used for the baseline model of transmission and reception [32]. Simulation parameters are summarized in Table 2. A uniform rectangular array (URA) of 16 antenna elements is used for the transmitter and uniform linear array (ULA) of eight elements for the receiver. UMi is used as the pathloss model and model B is used for blockage modeling. The performance of the beam-sweeping period and data transmission period are evaluated using the frame structure in Fig. 2.

Fig. 7 shows the signal strengths received from the BS and RS when the scenario (one BS and one RS) in Fig. 1 is applied. Here, an RS is assumed to be placed at a distance of 60 meters from the BS. The RS is assumed to have a gain of 30dB to overcome the pathloss between the BS and RS link. A single blockage is considered for simulation and the distance between the transmitter and blockage is changed randomly. The results in Fig. 7 show that the received signal power decreases as the distance between BS/RS and MS increases. When a blockage occurs between the BS(RS) and MS, 15−20 dB of power loss occurs in the BS(RS)-MS link.

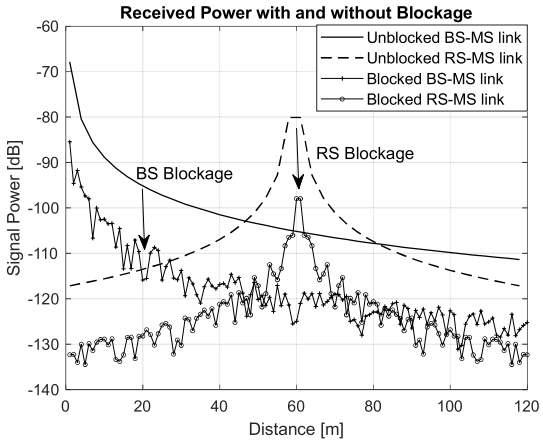

FIGURE 7. Received power with and without blockage.

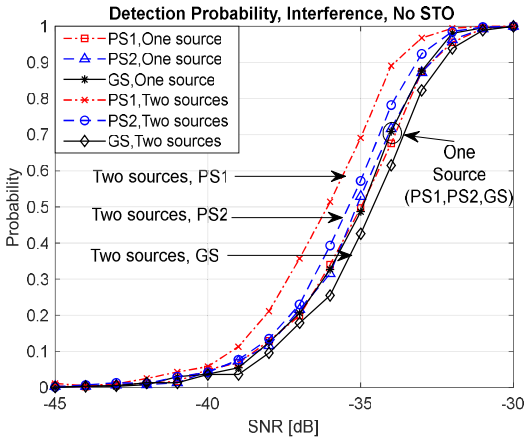

FIGURE 8. Detection probabilities of PS1, PS2, and GS when STO does not exist.

Fig. 8 shows the probability of detecting the beam-sweeping source when the link between the serving source (BS) and MS is blocked (Phase 2 in Fig. 1). The MS is assumed to be located 40 meters and 20 meters away from BS and RS, respectively. The pilot spacing (ρ) in the frequency domain is set to 32 subcarriers and the length of the pilot sequence is 127. Thus, the number of available pilot sequences for PS1 and PS2 is 127×126. It is also

assumed that STO does not exist between the RS and MS. Here, two different scenarios are considered: "one beam-sweeping source" and "two beam-sweeping sources." In the case of one beam-sweeping source, one RS (Phase 2 in Fig. 1) and in the case of two beam-sweeping sources, two RSs, of which the signals have the same power, are assumed to exist. The detection probability is obtained by correlating the received signal with reference pilot sequences and finding the sequence index with the largest correlation value, as given in (3) and (4). The detection is declared to be "successful" when the detected sequence index is correct. Fig. 8 shows that the performance of PS1, PS2, and GS is similar when only one beam-sweeping source is used. However, when two beam-sweeping sources are used, they interfere with each other. Because the cross-correlation property improves in the order of GS, PS2, and PS1 (Fig. 6 and Table 1), the probability of detection becomes higher in the same order (GS, PS2, and PS1). Although it is not shown here, the tendency of detection probability is similar when NID > 2.

In Fig. 8, the detection probability and the number of available pilot sequences are obtained under the assumption that STO does not exist between the RS and MS. Fig. 9 shows the detection probability of PS1 in the presence of STO because PS1 experiences the ambiguity problem when STO exists. Note that the sequence length (127) divided by the number of NIDs (2) is 63.5. Thus, G is 63 when the number of NIDs is 2. Fig. 9 shows that the sequence detection is correct when $\sigma = 0$ or 32, but wrong when $\sigma = 33$, in the case that the number of NIDs 2 and ρ is 32. The ambiguity in NID detection occurs when σ is larger than the maximum tolerable STO. When the pilot spacing (ρ) and the number of NIDs are set to 16 (8) and 2, respectively, the maximum tolerable STO is ± 65 (131). Fig. 9 indicates that the sequence detection fails when σ is larger than the maximum tolerable STO. The ambiguity problem decreases as the number of NIDs or pilot spacing is reduced. Thus, the number of NIDs in PS1 decreases significantly when the range of STO increases. For example, when the pilot spacing and the maximum STO are 32 and 32, respectively, the number of available NIDs is 2 in PS1. For the case of 15 NIDs, the detection probability approaches 0 when σ is 19. The maximum tolerable STO is 18 in this case.

Fig. 10 shows the detection probabilities of PS2 and GS in the presence of STO for the same scenario of "one beam-sweeping source" as in Fig. 9. The figure shows that PS2 and GS do not experience the ambiguity problem even with a large STO ($\sigma = 2{,}000$), corresponding to almost a half symbol. However, it can cause a discontinuous phase within the FFT window, resulting in ISI. Fig. 10 compares the performance of the proposed method (continuous phase) with that of the normal mode (discontinuous phase) when different STOs are used. Clearly, the performance degradation (discontinuous phase) caused by STO ($\sigma = 2{,}000$) can be compensated for by the proposed method (continuous phase), which obtains a gain of approximately 6 dB. In addition, the number of NIDs in PS1 and GS is not affected by the STO value.

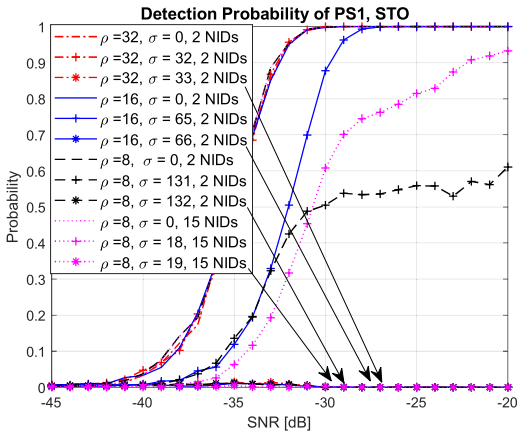

FIGURE 9. Detection probability of PS1 when STO exists.

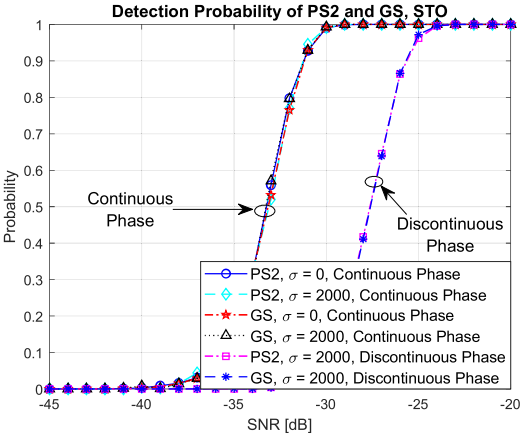

FIGURE 10. Detection probabilities of PS2 and GS when STO exists.

Fig. 11 shows the BER performance at the different phases in Fig. 2 when the proposed approach is successfully implemented. Here, it is also assumed that the MS is located 40 meters and 20 meters away from BS and RS, respectively. The best performance is obtained in Phase 1 where the MS is served by the BS. The performance in Phase 2 degrades by approximately 20 dB where a blockage occurs on the link between the BS and MS. In Phase 3, the gain is approximately 14 dB where the MS is served by the RS. The performance degradation in Phase 4 is approximately 15 dB where a blockage occurs on the link between the RS and MS. When the MS is again served by the BS (Phase 1), the gain is approximately 21 dB. The BER performance in Phase 1 is 6 dB higher than that in Phase 3 because the power received from the BS is 6 dB greater than that from the RS as shown in Fig. 7.

To compare the proposed technique with the conventional technique, we consider the existing cellular system where an RS is regarded as another BS with different CID. In the existing cellular system, the RS will follow the conventional initialization procedure to reestablish the link whenever a blockage occurs. Initial synchronization is achieved using the SSB defined in 3GPP specifications [35], [36]. The SSB is repeated after specific time (ranges from 5ms to 160ms depending on channel condition). When a blockage occurs,

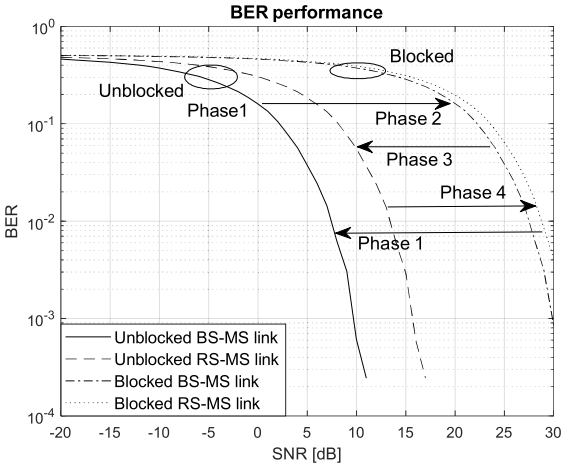

FIGURE 11. BER performances at different phases in Fig. 2.

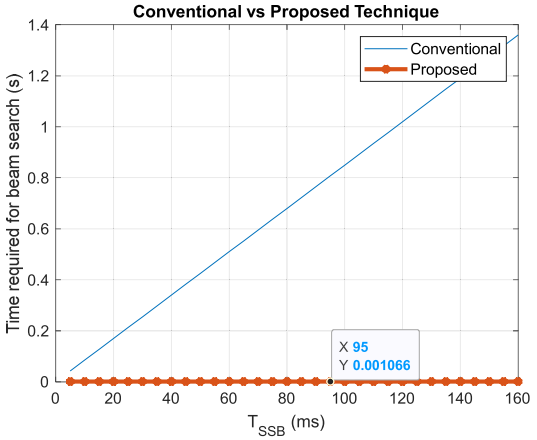

FIGURE 12. Time required for cell and beam search in conventional and proposed techniques.

the sweeping source will transmit four symbols of SSB during the SSB period. As defined in NR specification [32], the BS (or RS) can transmit the SSB on multiple transmit beams and the MS receives the signal using one beam. Here, we consider the best scenario for the conventional technique, where the SSB is transmitted simultaneously from all Tx beams. This procedure is repeated for all Rx beams in the MS. Thus, the time required for reestablishing the link in the conventional technique will be $O(T_{SSB} \times N_{Rx})$. Here, N_{Tx}, N_{Rx}, T_{SSB} and T_{sym} represent the number of Tx beams, number of Rx beams, SSB duration, and symbol duration. However, in the proposed technique, the link is reestablished using the received pilot signals, designed for RSs in mmWave cellular systems. Since the pilot signals are transmitted continuously from the sweeping source in the proposed technique, the required time for cell and beam search will be $O(N_{Tx} \times T_{sym} \times N_{Rx})$. Fig. 12 compares the time required for cell and beam search in conventional and proposed techniques. The parameters in Table 2 are used for simulation in Fig. 12. Here, it is assumed that a blockage is occurred at $T_{SSB}/2$. From this figure, it can be seen that the time required for cell and beam search increases linearly for the conventional technique while it remains constant ($N_{Tx} \times N_{Rx} \times T_{sym} = 16 \times 8 \times 8.334\mu s = 1.0667ms$) for the proposed technique. Thus, the proposed technique can significantly reduce the time for link reestablishment when a blockage occurs. On the other hand, the computational complexity increases as the number of IDs increases, because the MS performs correlation operation for all possible IDs of adjacent BSs and RSs.

V. CONCLUSION

This study proposes the operational concept and framework of a pilot-based RS-assisted mmWave cellular system to alleviate the blockage problem. Two different types of pilot sequences (PS1 and PS2), which can generate a large number of IDs with a low correlation, are proposed to allow MSs to distinguish the pilot sources in multi-cell multi-relay environments. PS1 was shown to have the smallest correlation and highest detection probability when the pilot signals transmitted from adjacent RSs/BSs arrive at the MS with small STOs. However, the detection probability of PS1 may decrease significantly when large STOs exist, due to the ambiguity in node detection. PS2 was proposed to increase the number of distinguishable IDs in the presence of STOs. PS2 with continuous phase was shown to experience no ambiguity problem with respect to node detection even with a large STO. Although pilot sequences were designed for mmWave cellular systems with one-hop relays in this study, the sequences could be used for any pilot-based cellular system that requires a large number of IDs with a low correlation.

APPENDIXES

APPENDIX A: PROOF OF PROPOSTION 1

From the "shift-and-add property" of the m-sequence, another m-sequence can be obtained by multiplying an m-sequence by its shifted version with an offset δ as follows:

$$p_{n-D_{\delta+\tau}} p_{n-D_{\delta+\tau}+\delta} = p_{n+D_\delta-D_{\delta+\tau}}. \tag{A.1}$$

If it is assumed that $(D_\delta - D_{\delta+\tau})_{\%N}$ can have the same value for two different values of δ (f and g), $p_{n+D_g-D_{g+\tau}}$, and $p_{n+D_f-D_{f+\tau}}$ must be the same and the following relationship must be hold ("shift-and-add property" of the m-sequence).

$$p_{n-D_{g+\tau}} p_{n-D_{g+\tau}+g} = p_{n-D_{f+\tau}} p_{n-D_{f+\tau}+f}. \tag{A.2}$$

If (18) is true, the correlation between the sequences on the right-hand side and left-hand side in (18) can be expressed as

$$\begin{aligned} N &= \sum_{n=0}^{N-1} \left(p_{n-D_{g+\tau}} p_{n-D_{g+\tau}+g}\right)\left(p_{n-D_{f+\tau}} p_{n-D_{f+\tau}+f}\right) \\ &= \sum_{n=0}^{N-1} \left(p_{n-D_{g+\tau}} p_{n-D_{g+\tau}+g}\right)\left(p_{n-D_{g+\tau}-\Delta} p_{n-D_{g+\tau}-\Delta+g+\theta}\right) \\ &= \sum_{n=0}^{N-1} p_{n-D_{g+\tau}+D_g} p_{n-D_{g+\tau}-\Delta+D_{g+\theta}}, \end{aligned} \tag{A.3}$$

where $D_{f+\tau}$ is $D_{g+\tau} + \Delta$, and f is $g + \theta$. If $D_{g+\theta} (= D_f)$ is $D_{g+\theta+\tau}$, (19) is true. However, $D_{g+\theta}$ cannot be $D_{g+\theta+\tau}$

within the range of τ from 1 to $N-1$, because D_δ has a different value for all shifts δ (''shift-and-add property'' of the m-sequence). Therefore, the assumption and (A.3) cannot be true, and the proposition is correct.

APPENDIX B: PROOF OF COROLLARY 1

From the ''shift-and-add property'' of the m-sequence, we can obtain another m-sequence by multiplying an m-sequence by its shifted version with an offset δ as follows:

$$p_n p_{n+\delta} = \begin{cases} p_{n+D_\delta}, & \text{when } n \text{ is the reference point} \\ p_{n+\delta+D_{-\delta}}, & \text{when } n+\delta \text{ is the reference point.} \end{cases} \tag{B.1}$$

Then, $\delta + D_{-\delta}$ and D_δ must be the same. Therefore, $D_\delta - D_{-\delta}$ is δ.

APPENDIX C: PROOF OF COROLLARY 2

It can be easily shown that $(D_\delta - D_{\delta+\tau})_{\%N}$ cannot be 0, because the values of D_δ are different for all values of δ(''shift-and-add property'' of the m-sequence) and τ has a non-zero value. Next, if $(D_\delta - D_{\delta+\tau})_{\%N}$ is equal to $N-\tau$, $(D_\delta - D_{\delta+\tau})_{\%N}$ becomes $(D_{N-\tau} - D_\tau)_{\%N}$ (Corollary 1). This assumption can be expressed as

$$(D_\delta - D_{N-\tau})_{\%N} = (D_{\delta+\tau} - D_\tau)_{\%N}. \tag{C.1}$$

However, (21) cannot be true because of Proposition 1. The term $(D_\delta - D_{\delta+\tau})_{\%N}$ must be different for different values of δ. Thus, $(D_\delta - D_{\delta+\tau})_{\%N}$ cannot be $N-\tau$ if δ has a value ranging from 1 to $N-1$ except $N-\tau$.

REFERENCES

[1] J. Zhang, X. Ge, Q. Li, M. Guizani, and Y. Zhang, ''5G millimeter-wave antenna array: Design and challenges,'' *IEEE Wireless Commun.*, vol. 24, no. 2, pp. 106–112, Apr. 2017.
[2] F. J. Martin-Vega, M. C. Aguayo-Torres, G. Gomez, J. T. Entrambasaguas, and T. Q. Duong, ''Key technologies, modeling approaches, and challenges for millimeter-wave vehicular communications,'' *IEEE Commun. Mag.*, vol. 56, no. 10, pp. 28–35, Oct. 2018.
[3] C. Zhang, W. Zhang, W. Wang, L. Yang, and W. Zhang, ''Research challenges and opportunities of UAV millimeter-wave communications,'' *IEEE Wireless Commun.*, vol. 26, no. 1, pp. 58–62, Feb. 2019.
[4] L. Wang, Y. L. Che, J. Long, L. Duan, and K. Wu, ''Multiple access mmWave design for UAV-aided 5G communications,'' *IEEE Wireless Commun.*, vol. 26, no. 1, pp. 64–71, Feb. 2019.
[5] H. Wymeersch, G. Seco-Granados, G. Destino, D. Dardari, and F. Tufvesson, ''5G mmWave positioning for vehicular networks,'' *IEEE Wireless Commun.*, vol. 24, no. 6, pp. 80–86, Dec. 2017.
[6] M. S. Elbamby, C. Perfecto, M. Bennis, and K. Doppler, ''Toward low-latency and ultra-reliable virtual reality,'' *IEEE Netw.*, vol. 32, no. 2, pp. 78–84, Mar./Apr. 2018.
[7] E. Bastug, M. Bennis, M. Medard, and M. Debbah, ''Toward interconnected virtual reality: Opportunities, challenges, and enablers,'' *IEEE Commun. Mag.*, vol. 55, no. 6, pp. 110–117, Jun. 2017.
[8] F. Jameel, S. Wyne, S. J. Nawaz, and Z. Chang, ''Propagation channels for mmWave vehicular communications: State-of-the-art and future research directions,'' *IEEE Wireless Commun.*, vol. 26, no. 1, pp. 144–150, Feb. 2019.
[9] S. Parkvall, E. Dahlman, A. Furuskar, and M. Frenne, ''NR: The new 5G radio access technology,'' *IEEE Commun. Standards Mag.*, vol. 1, no. 4, pp. 24–30, Dec. 2017.
[10] S.-Y. Lien, S.-L. Shieh, Y. Huang, B. Su, Y.-L. Hsu, and H.-Y. Wei, ''5G new radio: Waveform, frame structure, multiple access, and initial access,'' *IEEE Commun. Mag.*, vol. 55, no. 6, pp. 64–71, Jun. 2017.
[11] J.-C. Lin, ''Synchronization requirements for 5G: An overview of standards and specifications for cellular networks,'' *IEEE Veh. Technol. Mag.*, vol. 13, no. 3, pp. 91–99, Sep. 2018.
[12] A. Scaglione, D. L. Goeckel, and J. N. Laneman, ''Cooperative communications in mobile ad hoc networks,'' *IEEE Signal Process. Mag.*, vol. 23, no. 5, pp. 18–29, Sep. 2006.
[13] J. N. Laneman, D. N. C. Tse, and G. W. Wornell, ''Cooperative diversity in wireless networks: Efficient protocols and outage behavior,'' *IEEE Trans. Inf. Theory*, vol. 50, no. 12, pp. 3062–3080, Dec. 2004.
[14] H. Y. Wei, J. Rykowski, and S. Dixit, *WiFi, WiMAX, and LTE Multi-hop Mesh Networks: Basic Communication Protocols and Application Areas*. Hoboken, NJ, USA: Wiley, 2013.
[15] A. Toding, M. R. Khandaker, and Y. Rong, ''Joint source and relay optimization for parallel MIMO relay networks,'' *EURASIP J. Adv. Signal Process.*, vol. 2012, no. 1, pp. 1–7, Dec. 2012.
[16] B. Xie, Z. Zhang, and R. Q. Hu, ''Performance study on relay-assisted millimeter wave cellular networks,'' in *Proc. IEEE 83rd Veh. Technol. Conf. (VTC Spring)*, May 2016, pp. 1–5.
[17] Z. Lan, C.-S. Sum, J. Wang, T. Baykas, F. Kojima, H. Nakase, and H. Harada, ''Relay with deflection routing for effective throughput improvement in gbps millimeter-wave WPAN systems,'' *IEEE J. Sel. Areas Commun.*, vol. 27, no. 8, pp. 1453–1465, Oct. 2009.
[18] S. Biswas, S. Vuppala, J. Xue, and T. Ratnarajah, ''On the performance of relay aided millimeter wave networks,'' *IEEE J. Sel. Topics Signal Process.*, vol. 10, no. 3, pp. 576–588, Apr. 2016.
[19] G. Yang and M. Xiao, ''Performance analysis of millimeter-wave relaying: Impacts of beamwidth and self-interference,'' *IEEE Trans. Commun.*, vol. 66, no. 2, pp. 589–600, Feb. 2018.
[20] H. Abbas and K. Hamdi, ''Millimeter wave communications over relay networks,'' in *Proc. IEEE Wireless Commun. Netw. Conf. (WCNC)*, San Francisco, CA, USA, Mar. 2017, pp. 1–6.
[21] K. Belbase, C. Tellambura, and H. Jiang, ''Two-way relay selection for millimeter wave networks,'' *IEEE Commun. Lett.*, vol. 22, no. 1, pp. 201–204, Jan. 2018.
[22] X. Xue, Y. Wang, X. Wang, and T. E. Bogale, ''Joint source and relay precoding in multiantenna millimeter-wave systems,'' *IEEE Trans. Veh. Technol.*, vol. 66, no. 6, pp. 4924–4937, Jun. 2017.
[23] D. Jagyasi and P. Ubaidulla, ''In-band full-duplex relay-assisted millimeter-wave system design,'' *IEEE Access*, vol. 7, pp. 2291–2304, 2019.
[24] S. Wu, R. Atat, N. Mastronarde, and L. Liu, ''Improving the coverage and spectral efficiency of millimeter-wave cellular networks using device-to-device relays,'' *IEEE Trans. Commun.*, vol. 66, no. 5, pp. 2251–2265, May 2018.
[25] J. Deng, ''Millimeter-wave communication and mobile relaying in 5G cellular networks,'' Ph.D. dissertation, Dept. Commun. Netw., Aalto Univ., Espoo, Finland, 2018.
[26] V. K. Sakarellos, D. Skraparlis, A. D. Panagopoulos, and J. D. Kanellopoulos, ''Optimum placement of radio relays in millimeter-wave wireless dual-hop networks [wireless corner],'' *IEEE Antennas Propag. Mag.*, vol. 51, no. 2, pp. 190–199, Apr. 2009.
[27] L. Kong, L. Ye, F. Wu, M. Tao, G. Chen, and A. V. Vasilakos, ''Autonomous relay for millimeter-wave wireless communications,'' *IEEE J. Sel. Areas Commun.*, vol. 35, no. 9, pp. 2127–2136, Sep. 2017.
[28] J. D. Oliva Sanchez and J. I. Alonso, ''A two-hop MIMO relay architecture using LTE and millimeter wave bands in high-speed trains,'' *IEEE Trans. Veh. Technol.*, vol. 68, no. 3, pp. 2052–2065, Mar. 2019.
[29] M. S. Elbamby, C. Perfecto, M. Bennis, and k. doppler, ''Toward low-latency and ultra-reliable virtual reality,'' *IEEE Netw.*, vol. 32, no. 2, pp. 78–84, Mar./Apr. 2018.
[30] Y. S. Cho, *MIMO-OFDM Wireless Communications With MATLAB*. Hoboken, NJ, USA: Wiley, 2010.
[31] H. Zerpernick and A. Finger, *Pseudo Random Signal Processing: Theory and Application*. Hoboken, NJ, USA: Wiley, 2005.
[32] *Study on Channel Model for Frequencies from 0.5 to 100 GHz (Release 14), Technical Specification Group Radio Access Network*, document TR 38.901, V14.2.0, 3rd Generation Partnership Project, Sep. 2017.
[33] *METIS Channel Models, Version 1.0*, document ICT-317669-METIS/D1.4, Feb. 2015.
[34] Y. Lin, '''Shift and add' property of m-sequences and its application to channel characterisation of digital magnetic recording,'' *IEE Proc. Commun.*, vol. 142, no. 3, pp. 135–140, Jun. 1995.

[35] *NR Physical Channels and Modulation (Release 16), Technical Specification Group Radio Access Network*, document TS 38.2111v16.0.0, 3rd Generation Partnership Project, Feb. 2019.
[36] E. Dahalman, S. Parkvall, and J. Skold, *5G NR: The Next Generation Wireless Access Technology*. Amsterdam, The Netherlands: Elsevier, 2018.

YEONG JUN KIM was born in South Korea, in 1981. He received the B.S., M.S., and Ph.D. degrees in electrical and electronics engineering from Chung-Ang University, Seoul, South Korea, in 2005, 2007, and 2011, respectively.

From 2005 to 2011, he was a Research Assistant with the Mobile Communications Laboratory, Chung-Ang University. From 2011 to 2015, he worked at LIG NEX1, South Korea, as a Senior Research Engineer. He was involved in developing modems for multiband and multirole radio. Since 2015, he has been working as the Deputy Principal Research Engineer with LG Electronics Company, Seoul. He has been involved in standardization of 5G NR and development of MODEM chipset for LTE-A and 5G. He is the author of more than 50 conference and articles. His research interests include the area of mobile communication and digital signal processing, especially for MIMO-OFDM and 5G.

QASIM SULTAN was born in Pakistan, in 1994. He received the B.S. degree in electrical and telecommunications engineering from COMSATS University, Islamabad, Pakistan, in 2017, and the M.S. degree in electrical and electronics engineering from Chung-Ang University, Seoul, South Korea, in 2019, where he is currently pursuing the Ph.D. degree in electrical and electronics engineering.

Since 2017, he has been working as a Research Assistant with the Mobile Communications Laboratory, Chung-Ang University. His research interest includes areas of wireless communication systems and digital signal processing. He was a recipient of Chung-Ang University Young Scientist Scholarship (CAYSS).

YONG SOO CHO (Senior Member, IEEE) was born in South Korea. He received the B.S. degree in electronics engineering from Chung-Ang University, Seoul, South Korea, in 1984, the M.S. degree in electronics engineering from Yonsei University, Seoul, in 1987, and the Ph.D. degree in electrical and computer engineering from the University of Texas, Austin, TX, USA, in 1991.

In 1984, he was a Research Engineer with Goldstar Electrical Company, Osan, South Korea. Since 1992, he has been a Professor with the School of Electrical and Electronics Engineering, Chung-Ang University. In 2001, he was a Visiting Research Fellow with the Electronics and Telecommunications Research Institute. He is the author of 12 books, more than 400 conference and articles, and more than 120 patents. His research interests include the area of mobile communication and digital signal processing, especially for MIMO OFDM and 5G.

Dr. Cho has served as the President of the Korean Institute of Communications and Information Sciences, in 2016, and was a recipient of Dr. Irwin Jacobs Award, in 2013.